J|A|C|S ARTICLES

Published on Web 01/16/2009

Accurate Measurement of Alpha Proton Chemical Shifts of Excited Protein States by Relaxation Dispersion NMR Spectroscopy

Patrik Lundström, D. Flemming Hansen, Pramodh Vallurupalli, and Lewis E. Kay*

Departments of Molecular Genetics, Biochemistry and Chemistry, The University of Toronto, Toronto, Ontario, Canada, M5S 1A8

Received October 2, 2008; E-mail: kay@pound.med.utoronto.ca

Abstract: Carr−Purcell−Meiboom−Gill relaxation dispersion NMR spectroscopy can provide detailed information about low populated, invisible states of protein molecules, including backbone chemical shifts of the invisible conformer and bond vector orientations that can be used as structural constraints. Notably, the measurement of $^1H^\alpha$ chemical shifts in excited protein states has not been possible to date because, in the absence of suitable labeling, the homonuclear proton scalar coupling network in side chains of proteins leads to a significant degradation in the performance of proton-based relaxation dispersion experiments. Here we have overcome this problem through a labeling scheme in which proteins are prepared with U−^{2}H glucose and 50% D_2O/50% H_2O that results in deuteration levels of between 50−88% at the C^β carbon. Effects from residual $^1H^\alpha-^1H^\beta$ scalar couplings can be suppressed through a new NMR experiment that is presented here. The utility of the methodology is demonstrated on a ligand binding exchanging system and it is shown that $^1H^\alpha$ chemical shifts extracted from dispersion profiles are, on average, accurate to 0.03 ppm, an order of magnitude better than they can be predicted from structure using a database approach. The ability to measure $^1H^\alpha$ chemical shifts of invisible conformers is particularly important because such shifts are sensitive to both secondary and tertiary structure. Thus, the methodology presented is a valuable addition to a growing list of experiments for characterizing excited protein states that are difficult to study using the traditional techniques of structural biology.

Introduction

NMR spectroscopy is a powerful technique for studying molecular dynamics over a wide range of time-scales, and new approaches are continually emerging.[1−4] In the past several years, there has been significant progress in the development of NMR methods for characterizing millisecond time-scale motions in proteins that are often of relevance for a wide variety of biological processes. Particularly exciting has been the development of Carr−Purcell−Meiboom−Gill (CPMG) relaxation dispersion experiments[5,6] that can be used to study exchange processes involving the interconversion of a highly populated (ground) state and low populated, transiently formed (excited) states.[7,8] The low population and transient nature of these states often renders them invisible to most biophysical methods. Yet their presence can be established quite readily in NMR spectra through increased broadening of peaks that derive from the visible ground state. This excess broadening, in turn, can be manipulated in CPMG experiments where transverse relaxation rates, $R_{2,\mathrm{eff}}$, are measured as a function of the repetition rate of refocusing pulses, ν_{CPMG}, during a constant-time relaxation delay.[9,10] The resulting dependence is then fit to the appropriate model to extract the kinetics and thermodynamics of the exchange process as well as the chemical shift differences between the exchanging states.[11−13] Applications to protein folding,[14−17] enzyme catalysis[18−23] and ligand binding[17,24] have

(1) Peng, J. W.; Wagner, G. *Methods Enzymol.* **1994**, *239*, 563–596.
(2) Ishima, R.; Torchia, D. A. *Nat. Struct. Biol.* **2000**, *7*, 740–743.
(3) Palmer, A. G.; Williams, J.; McDermott, A. *J. Phys. Chem.* **1996**, *100*, 13293–13310.
(4) Mittermaier, A.; Kay, L. E. *Science* **2006**, *312*, 224–228.
(5) Carr, H. Y.; Purcell, E. M. *Phys. Rev.* **1954**, *94*, 630–638.
(6) Meiboom, S.; Gill, D. *Rev. Sci. Instrum.* **1958**, *29*, 688–691.
(7) Palmer, A. G., III; Kroenke, C. D.; Loria, J. P. *Methods Enzymol.* **2001**, *339*, 204–238.
(8) Palmer, A. G.; Grey, M. J.; Wang, C. Y. *Methods Enzymol.* **2005**, *394*, 430–465.
(9) Loria, J. P.; Rance, M.; Palmer, A. G., III *J. Am. Chem. Soc.* **1999**, *121*, 2331–2332.
(10) Tollinger, M.; Skrynnikov, N. R.; Mulder, F. A. A.; Forman-Kay, J. D.; Kay, L. E. *J. Am. Chem. Soc.* **2001**, *123*, 11341–11352.
(11) Bloch, F. *Phys. Rev.* **1946**, *70*, 460–474.
(12) McConnell, H. M. *J. Chem. Phys.* **1958**, *28*, 430–431.
(13) Carver, J. P.; Richards, R. E. *J. Magn. Reson.* **1972**, *6*, 89–&.
(14) Hill, R. B.; Bracken, C.; DeGrado, W. F.; Palmer, A. G. *J. Am. Chem. Soc.* **2000**, *122*, 11610–11619.
(15) Korzhnev, D. M.; Salvatella, X.; Vendruscolo, M.; Di Nardo, A. A.; Davidson, A. R.; Dobson, C. M.; Kay, L. E. *Nature* **2004**, *430*, 586–590.
(16) Zeeb, M.; Balbach, J. *J. Am. Chem. Soc.* **2005**, *127*, 13207–13212.
(17) Sugase, K.; Dyson, H. J.; Wright, P. E. *Nature* **2007**, *447*, 1021–1025.
(18) Eisenmesser, E. Z.; Bosco, D. A.; Akke, M.; Kern, D. *Science* **2002**, *295*, 1520–1523.
(19) Eisenmesser, E. Z.; Millet, O.; Labeikovsky, W.; Korzhnev, D. M.; Wolf-Watz, M.; Bosco, D. A.; Skalicky, J. J.; Kay, L. E.; Kern, D. *Nature* **2005**, *438*, 117–121.
(20) Wolf-Watz, M.; Thai, V.; Henzler-Wildman, K.; Hadjipavlou, G.; Eisenmesser, E. Z.; Kern, D. *Nat. Struct. Mol. Biol.* **2004**, *11*, 945–949.
(21) Boehr, D. D.; McElheny, D.; Dyson, H. J.; Wright, P. E. *Science* **2006**, *313*, 1638–1642.

emerged in the past several years, and detailed information about excited states can often be obtained despite the fact that in many cases they cannot be observed directly.

One of the most important features of the CPMG dispersion experiment is that it is sensitive to chemical shift differences between the interconverting states and hence the chemical shifts of the excited state. Indeed excited-state shifts can be obtained from a combined analysis of dispersion data and simple two-dimensional heteronuclear correlation maps that are recorded at a number of static magnetic fields, as described previously by Skrynnikov et al.[25] The resultant chemical shifts can, in turn, be used as probes of structure—in this case, of excited states that are recalcitrant to direct observation.

The chemical shifts of $^{13}C^{\alpha}$, $^{13}C^{\beta}$, ^{13}CO, ^{15}N, ^{1}HN and $^{1}H^{\alpha}$ nuclei are now routinely used in NMR structure calculations of 'populated ground states' by 'converting them' into dihedral angle restraints[26] that complement nuclear Overhauser enhancements (NOE) and residual dipolar coupling (RDC) restraints.[27−30] Recently it has been shown that these shifts can be used as the sole experimental restraints in database structure determination protocols to produce structures that agree well with those generated using 'traditional' NMR or X-ray based methods so long as the proteins are of moderately small size (≤150 residues).[31,32] In a related application our laboratory has recently presented the backbone fold of an invisible, excited-state that corresponds to the peptide bound form of the Abp1p SH3 domain[33] using restraints that were exclusively derived from relaxation dispersion data. These include (ϕ,ψ) restraints that were obtained using the database program TALOS[26] from ^{15}N, $^{1}H^{N}$, $^{13}C^{\alpha}$ and ^{13}CO chemical shifts[34] of the excited-state and anisotropic restraints in the form of $^{1}HN-^{15}N$,[35] $^{1}H^{\alpha}-^{13}C^{\alpha}$, $^{1}HN-^{13}CO$ RDCs[36] and changes in ^{13}CO chemical shifts upon alignment (^{13}CO RCSAs)[37] that were measured for the excited-state using spin-state selective relaxation dispersion experiments.

One obvious omission in the list of chemical shifts of the excited-state that have been measured to date is that of $^{1}H^{\alpha}$. Although its chemical shift is an indicator of secondary structure like $^{13}C^{\alpha}$, $^{13}C^{\beta}$ and ^{13}CO shifts[38−40] the $^{1}H^{\alpha}$ shift is complementary since it is also sensitive to ring currents[41−43] and hydrogen bonding.[44,45] $^{1}H^{\alpha}$ chemical shifts extend from approximately 3.0 − 6.0 ppm, while random coil α-proton shifts range over ∼0.75 ppm or 25% of the total variation in $^{1}H^{\alpha}$ chemical shift space.[43] Thus, the chemical shift of $^{1}H^{\alpha}$ is extremely sensitive to structure. Much of this sensitivity is derived from the exquisite dependence on the dihedral angels ϕ_i/ψ_i that can cause the secondary chemical shift to be perturbed downfield by 0.7 ppm and upfield by 0.6 ppm for extended and helical conformations respectively.[43] Most important, the $^{1}H^{\alpha}$ chemical shift is also particularly sensitive to ring current effects of nearby aromatic rings and these can cause upfield or downfield variations of as much as 1.5 ppm.[43] Thus measurement of $^{1}H^{\alpha}$ shifts provides tertiary information as well. Additional effects that contribute to the shift range include hydrogen bonding to oxygen of carbonyl groups on opposite β-strands,[44] although this effect largely is accounted for by the ϕ_i/ψ_i dependence,[42] interactions with solvent and proximal charges. Known structural effects account for almost all of the $^{1}H^{\alpha}$ chemical shift and indeed, the program SPARTA can predict it very well, to within an rmsd of 0.27 ppm for known structures.[42] Since the $^{1}H^{\alpha}$ chemical shift can be predicted accurately, it is clearly useful to include it in structure calculations.

The measurement of $^{1}H^{\alpha}$ chemical shifts of excited protein states using relaxation dispersion methods, has to this point been problematic, however. In applications involving protonated molecules the transfer of magnetization between scalar coupled proton spins that is facilitated by ^{1}H refocusing pulses during the CPMG period leads to artifacts in dispersion profiles that significantly complicate the extraction of robust exchange parameters. Here we circumvent this problem by developing a labeling scheme in which proteins are expressed in 50% D_2O, using uniformly deuterated and ^{13}C-labeled glucose as the carbon source, which eliminates many of the unwanted $^{1}H-^{1}H$ scalar couplings. Further, an $^{1}H^{\alpha}$ dispersion pulse scheme is presented that to a large extent refocuses evolution from the remaining proton scalar couplings. It is shown that the combination of the new labeling protocol and the new $^{1}H^{\alpha}$ dispersion experiment permits the measurement of accurate $^{1}H^{\alpha}$ chemical shift differences linking the ground and excited states. The addition of $^{1}H^{\alpha}$ shifts to the list of those that are presently quantified by relaxation dispersion will lead to an improved description of the structures of low populated, invisible conformers.

Materials and Methods

Protein Sample Preparation. Samples of the Abp1p SH3 domain[46−48] were prepared with isotopic enrichment by protein expression in BL21(DE3) cells grown in M9 minimal media, 50% D_2O, supplemented with 1 g/L $^{15}NH_4Cl$ and 3 g/L [$^{13}C_6$,$^{2}H_7$]-glucose as the sole nitrogen and carbon sources, respectively. Cells were grown to OD 0.8 and protein expression induced with 1 mM IPTG.

(22) Watt, E. D.; Shimada, H.; Kovrigin, E. L.; Loria, J. P. *Proc. Natl. Acad. Sci. U.S.A.* **2007**, *104*, 11981–11986.
(23) Vallurupalli, P.; Kay, L. E. *Proc. Natl. Acad. Sci. U.S.A.* **2006**, *103*, 11910–11915.
(24) Mulder, F. A. A.; Mittermaier, A.; Hon, B.; Dahlquist, F. W.; Kay, L. E. *Nat. Struct. Biol.* **2001**, *8*, 932–935.
(25) Skrynnikov, N. R.; Dahlquist, F. W.; Kay, L. E. *J. Am. Chem. Soc.* **2002**, *124*, 12352–12360.
(26) Cornilescu, G.; Delaglio, F.; Bax, A. *J. Biomol. NMR* **1999**, *13*, 289–302.
(27) Tjandra, N.; Bax, A. *Science* **1997**, *278*, 1111–1114.
(28) Tolman, J. R.; Flanagan, J. M.; Kennedy, M. A.; Prestegard, J. H. *Proc. Natl. Acad. Sci. U.S.A.* **1995**, *92*, 9279–9283.
(29) Bax, A. *Protein Sci.* **2003**, *12*, 1–16.
(30) Prestegard, J. H.; Mayer, K. L.; Valafar, H.; Benison, G. C. *Methods Enzymol.* **2005**, *394*, 175–209.
(31) Shen, Y.; et al. *Proc. Natl. Acad. Sci. U.S.A.* **2008**, *105*, 4685–4690.
(32) Cavalli, A.; Salvatella, X.; Dobson, C. M.; Vendruscolo, M. *Proc. Natl. Acad. Sci. U.S.A.* **2007**, *104*, 9615–9620.
(33) Vallurupalli, P.; Hansen, D. F.; Kay, L. E. *Proc. Natl. Acad. Sci. U.S.A.* **2008**, *105*, 11766–11771.
(34) Hansen, D. F.; Vallurupalli, P.; Lundström, P.; Neudecker, P.; Kay, L. E. *J. Am. Chem. Soc.* **2008**, *130*, 2667–2675.
(35) Vallurupalli, P.; Hansen, D. F.; Stollar, E.; Meirovitch, E.; Kay, L. E. *Proc. Natl. Acad. Sci. U.S.A.* **2007**, *104*, 18473–18477.
(36) Hansen, D. F.; Vallurupalli, P.; Kay, L. E. *J. Am. Chem. Soc.* **2008**, *130*, 8397–8405.
(37) Vallurupalli, P.; Hansen, D. F.; Kay, L. E. *J. Am. Chem. Soc.* **2008**, *130*, 2734–2735.
(38) Szilagyi, L. *Prog. Nucl. Magn. Reson. Spectrosc.* **1995**, *27*, 325–443.
(39) Spera, S.; Bax, A. *J. Am. Chem. Soc.* **1991**, *113*, 5490–5492.
(40) Wishart, D. S.; Sykes, B. D. *J. Biomol. NMR* **1994**, *4*, 171–180.
(41) Neal, S.; Nip, A. M.; Zhang, H. Y.; Wishart, D. S. *J. Biomol. NMR* **2003**, *26*, 215–240.
(42) Shen, Y.; Bax, A. *J. Biomol. NMR* **2007**, *38*, 289–302.
(43) Wishart, D. S.; Case, D. A. *Methods Enzymol.* **2002**, *338*, 3–34.
(44) Wagner, G.; Pardi, A.; Wuthrich, K. *J. Am. Chem. Soc.* **1983**, *105*, 5948–5949.
(45) Pardi, A.; Wagner, G.; Wuthrich, K. *Eur. J. Biochem.* **1983**, *137*, 445–454.
(46) Rath, A.; Davidson, A. R. *Protein Sci.* **2000**, *9*, 2457–2469.
(47) Lila, T.; Drubin, D. G. *Mol. Biol. Cell* **1997**, *8*, 367–385.
(48) Drubin, D. G.; Mulholland, J.; Zhu, Z. M.; Botstein, D. *Nature* **1990**, *343*, 288–290.

Overexpression was carried out at 37 °C for 7 h. A 17 residue peptide from the protein Ark1p[49] (primary sequence: KKTKPTPPPKPSHLKPK) was expressed as described previously.[35] The Abp1p SH3 domain and the unlabeled Ark1p peptide were purified according to Vallurupalli et al.[35] Samples were prepared in 50 mM sodium phosphate, 100 mM NaCl, 2 mM EDTA, and 2 mM NaN_3, pH 7.0 buffer, 100% D_2O. An exchanging $P + L \leftrightarrow PL$ sample was prepared by titrating Ark1p peptide into a solution of the SH3 domain so that [PL]/([P]+[PL]) ≈ 5% with a protein concentration of 1.4 mM (in the following referred to as the "5% bound sample"). A second sample with [PL]/([P]+[PL]) ≈ 95% and a protein concentration of 1.1 mM was also prepared (referred to as the "95% bound sample").

NMR Spectroscopy. All NMR experiments were performed at 25 °C on Varian Inova spectrometers with ^{1}H resonance frequencies of 500, 600 and 800 MHz, equipped with cold (600 MHz) and room temperature (500, 800 MHz) probe-heads.

Quantification of $C^\beta H^\beta_2$ isotopomer levels (or $C^\beta H^\beta$ for Ile, Thr and Val; $C^\beta H^\beta_3$ for Ala) in proteins prepared as described above was carried out to provide experimental verification of the predicted isotopomer distributions based on analysis of the appropriate metabolic pathways. This was done by recording deuterium decoupled constant-time ^{13}C HSQCs[50,51] on the sample of interest (prepared with U−^{13}C,^{2}H glucose and 50% D_2O) and on a uniformly ^{1}H/^{13}C/^{15}N sample and calculating the fraction of the fully protonated isotopomer as $f = (B_F/2\bar{A}_F)/(B_U/\bar{A}_U)$, where B_F and B_U are the intensities of a particular $^{13}C^\beta$,$^1H^\beta$ cross-peak (derived from a fully protonated C^β) in spectra recorded on the fractionally deuterated and uniformly protonated samples respectively and $\bar{A}_F$ and $\bar{A}_U$ are the average intensities of $^{13}C^\alpha$,$^1H^\alpha$ correlations in the spectra of the two samples that are used to normalize for different protein concentrations. The factor of 2 in the expression takes into account the fact that the intensities of the $^{13}C^\alpha$,$^1H^\alpha$ peaks are reduced by a factor of 2 in the fractionally deuterated sample since it is grown on 50% D_2O.[52]

$^1H^\alpha$ relaxation dispersion experiments were recorded at 600 (or 500) and 800 MHz on samples comprised of fractionally deuterated U−^{15}N, U−^{13}C Abp1p SH3 domains, 5% or 95% unlabeled Ark1p peptide using both versions of the pulse sequence described in Figure 2. Data sets recorded with the 5% bound sample were obtained with T_{relax}=30 ms, ν_{CPMG} values between 67 and 1000 Hz (N even) (see Figure 2), while data sets with the 95% bound sample were recorded T_{relax}=30 ms, values of ν_{CPMG} between 67 and 1333 Hz and even values for N. In all cases a total of 14 2D planes were recorded and the total experimental time for each complete dispersion data set was 24 and 31 h at 600 and 800 MHz respectively, while a measurement time of 48 h was used for the data set recorded at 500 MHz to compensate for the lower sensitivity of data recorded at this field.

Data sets were processed and analyzed with the nmrPipe/nmrDraw suite of programs[53] and peaks integrated using the program FuDA (available upon request). CPMG relaxation dispersion profiles, $R_{2,eff}(\nu_{CPMG})$ vs ν_{CPMG}, were calculated as $R_{2,eff}(\nu_{CPMG}) = -\ln(I(\nu_{CPMG})/I_0)/T_{relax}$, where $I(\nu_{CPMG})$ is the peak intensity for different ν_{CPMG} values and I_0 is the peak intensity obtained when the CPMG block is omitted. Here $\nu_{CPMG} = 1/(4\tau_{CP})$, where $2\tau_{CP}$ is the interval between successive 180° refocusing pulses during the CPMG element. Uncertainties in $R_{2,eff}(\nu_{CPMG})$ values were estimated from duplicate measurements. All dispersion data were fitted to a two-state model of chemical exchange to extract the global exchange rate, $k_{ex} = k_{on}[L] + k_{off}$, the population of the minor state, p_B, and residue specific chemical shift differences between the major and minor states, $\Delta\varpi$ (absolute values only). In order to establish which residues should be included in such fits, all dispersion profiles were initially fit on a per-residue basis to models that either include or do not include chemical exchange. Residues were retained for further analysis if fits using the two-site exchange model were significant as established by F-test analyses, with $p < 0.001$.

Results and Discussion

Problem with Measurement of $^1H^\alpha$ Chemical Shifts in Protonated Proteins via Relaxation Dispersion. The measurement of accurate $^1H^\alpha$ relaxation rates as a function of the number of refocusing pulses applied during the CPMG element is complicated in applications involving protonated proteins by evolution due to $^1H^\alpha-^1H^N$ and $^1H^\alpha-^1H^\beta$ scalar couplings that are not refocused during the CPMG pulse train and by additional couplings that relay magnetization transferred to $^1H^\beta$ to points further along the side-chain. Similar issues have been noted by Ishima and Torchia in ^{1}HN CPMG dispersion studies of protonated proteins, although in this case homonuclear scalar couplings can be eliminated through perdeuteration,[54]an option this is clearly not available presently. In the case of $^1H^\alpha$ relaxation studies, the amide proton can trivially be replaced by deuterium by recording the experiments in D_2O rather than in H_2O, however, the scalar coupling to $^1H^\beta$ with consensus values of 10.8 and 3.3 Hz for the trans and gauche χ^1 rotameric states respectively,[55] remains. To appreciate the problems that this can cause, consider the evolution of transverse $^1H^\alpha$ magnetization that is scalar coupled to a single $^1H^\beta$ proton (coupling constant of $J_{\alpha\beta}$) during the course of a CPMG pulse train where relaxation and pulse imperfections are neglected. In what follows we denote magnetization derived from α and β protons by I^α and I^β, respectively, and consider the evolution of $^1H^\alpha$ Y-magnetization, I^α_Y, in a number of limiting cases.

Simulations establish that in the slow pulsing limit, $|\Delta\omega\tau_{CP}| > \approx 2.5$ where $\Delta\omega$ is the difference between $^1H^\alpha$ and $^1H^\beta$ resonance frequencies and τ_{CP} is half the time between successive refocusing pulses in the CPMG pulse train, evolution of I^α_Y for a time T, proceeds according to

$$I^\alpha_Y \rightarrow I^\alpha_Y \cos(\pi J_{\alpha\beta} T) - 2I^\alpha_X I^\beta_Z \sin(\pi J_{\alpha\beta} T) \quad (1)$$

as expected in the weak scalar coupling limit. In contrast, in the rapid pulsing limit, $|\Delta\omega\tau_{CP}| < 1$, the evolution approaches that obtained in the strong coupling limit

$$I^\alpha_Y \rightarrow I^\alpha_Y \cos^2(\pi J_{\alpha\beta} T) + I^\beta_Y \sin^2(\pi J_{\alpha\beta} T) + (I^\alpha_Z I^\beta_X - I^\alpha_X I^\beta_Z) \sin(2\pi J_{\alpha\beta} T) \quad (2)$$

(49) Haynes, J.; Garcia, B.; Stollar, E. J.; Rath, A.; Andrews, B. J.; Davidson, A. R. *Genetics* **2007**, *176*, 193–208.
(50) Vuister, G. W.; Bax, A. *J. Magn. Reson.* **1992**, *98*, 428–435.
(51) Santoro, J.; King, G. C. *J. Magn. Reson.* **1992**, *97*, 202–207.
(52) Voet, D.; Voet, J. G. *Biochemistry*, 3rd ed.; John Wiley & Sons, Inc.: Hoboken, 1995.
(53) Delaglio, F.; Grzesiek, S.; Vuister, G. W.; Zhu, G.; Pfeifer, J.; Bax, A. *J. Biomol. NMR* **1995**, *6*, 277–293.
(54) Ishima, R.; Torchia, D. A. *J. Biomol. NMR* **2003**, *25*, 243–248.
(55) Perez, C.; Lohr, F.; Ruterjans, H.; Schmidt, J. M. *J. Am. Chem. Soc.* **2001**, *123*, 7081–7093.
(56) Rose, I. A.; O'Connell, E. L. *J. Biol. Chem.* **1961**, *236*, 3086–3092.
(57) Lundström, P.; Hansen, D. F.; Kay, L. E. *J Biomol NMR* **2008**, *42*, 35–47.
(58) Grzesiek, S.; Kuboniwa, H.; Hinck, A. P.; Bax, A. *J. Am. Chem. Soc.* **1995**, *117*, 5312–5315.
(59) Kupce, E.; Wagner, G. *J. Magn. Reson., Ser. B* **1995**, *109*, 329–333.
(60) Kupce, E.; Freeman, R. *J. Magn. Reson., Ser. A* **1995**, *117*, 246–256.
(61) Zhang, S. M.; Gorenstein, D. G. *J. Magn. Reson.* **1998**, *132*, 81–87.
(62) Shaka, A. J.; Keeler, J.; Frenkiel, T.; Freeman, R. *J. Magn. Reson.* **1983**, *52*, 335–338.
(63) States, D. J.; Haberkorn, R. A.; Ruben, D. J. *J. Magn. Reson.* **1982**, *48*, 286–292.
(64) Marion, D.; Ikura, M.; Tschudin, R.; Bax, A. *J. Magn. Reson.* **1989**, *85*, 393–399.
(65) Kupce, E.; Freeman, R. *J. Magn. Reson., Ser. A* **1995**, *115*, 273–276.

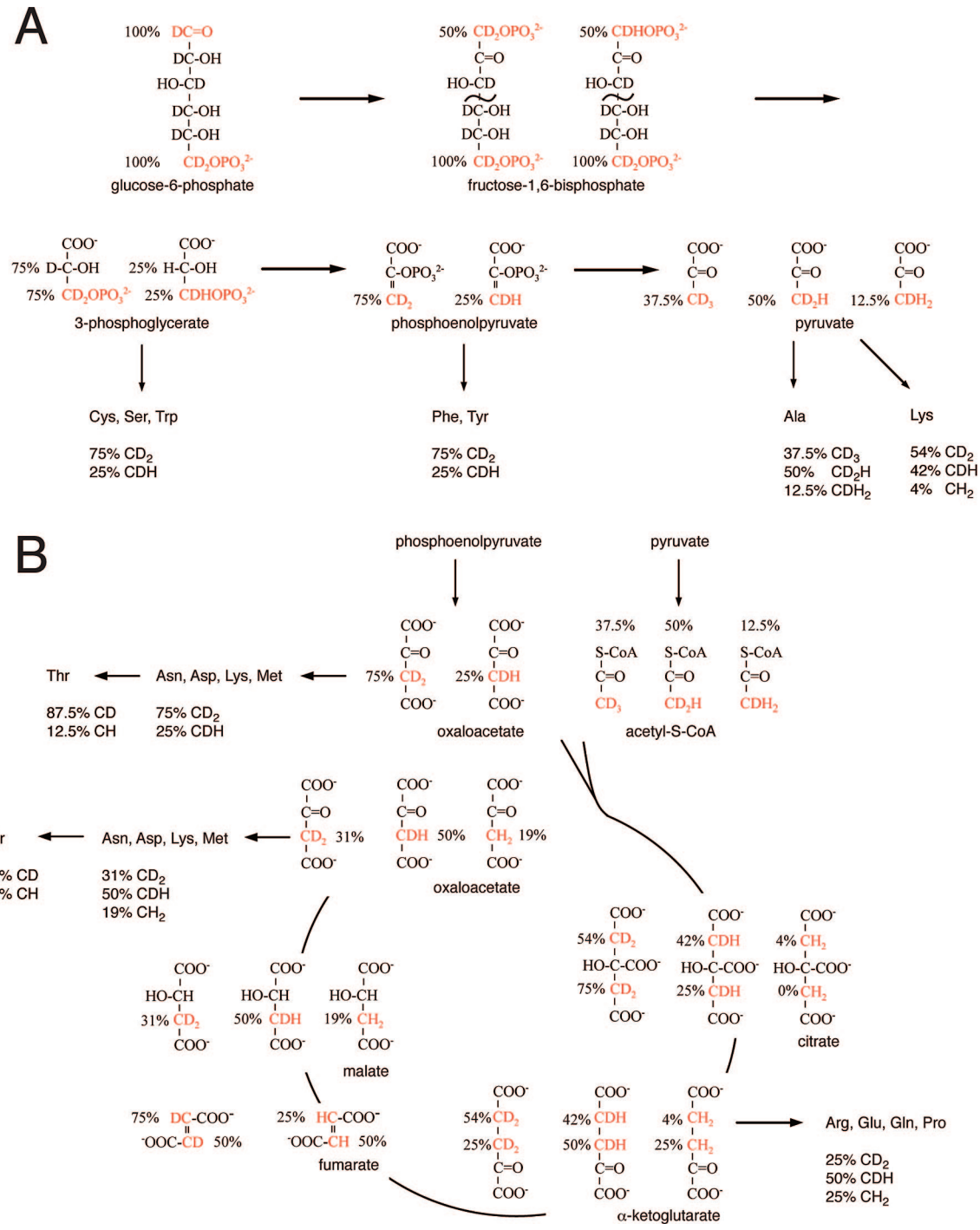

Figure 1. Pathways involved in the biosynthesis of the majority of the amino acids, with the isotopomer composition of several intermediates of glycolysis and the TCA cycle indicated, assuming a carbon source that is uniformly deuterated glucose and a solvent composition of 50% D_2O/50% H_2O. Positions that are precursors of C^{β} of the amino acids are colored red and the percentage of each isotopomer is indicated. Also shown are the derived amino acids and their isotopomer composition at the β-position. Amino acids, for which the β-position may originate from different precursors or for which the precursor can be synthesized in more than one way, are shown more than once. (A) Glycolysis and the amino acids derived from this pathway. For clarity, certain steps have been omitted. Note that for 3-phosphoglycerate the level of deuterium incorporation at each of the two hydrogen containing carbon sites is independent of the other. (B) The TCA cycle and the amino acids that are produced from TCA precursors. Only selected steps are shown. For citrate, α-ketoglutarate and fumarate the incorporation of deuterium at each of the two positions indicated in red is independent of the other.

The key measurable in the $^1H^{\alpha}$ dispersion experiment is the dependence of $^1H^{\alpha}$ magnetization on the number of pulses (and hence on τ_{CP}) that are applied during a fixed interval in time, T. The requirement is that in the absence of chemical exchange there is no dependence of magnetization intensity on τ_{CP} so that flat dispersions will be obtained. However, this is clearly not the case here. In the weak pulsing limit $^1H^{\alpha}$ Y-magnetization is attenuated by the factor $\cos(\pi J_{\alpha\beta}T)$ and this factor approaches $\cos^2(\pi J_{\alpha\beta}T)$ as $|\Delta\omega\tau_{CP}| < 1$. For example, consider the case where $\Delta\omega$ is 6300 s^{-1} (2.0 ppm at 500 MHz). Evolution is in the slow pulsing limit for $\nu_{CPMG} = 1/(4\tau_{CP}) < 630$ Hz, while for 630 Hz $< \nu_{CPMG} <$ 1575 Hz the value of $|\Delta\omega\tau_{CP}|$ varies between 1 and 2.5, with $|\Delta\omega\tau_{CP}|<1$ for $\nu_{CPMG} > 1575$ Hz. Thus, over the range of ν_{CPMG} values that are normally considered

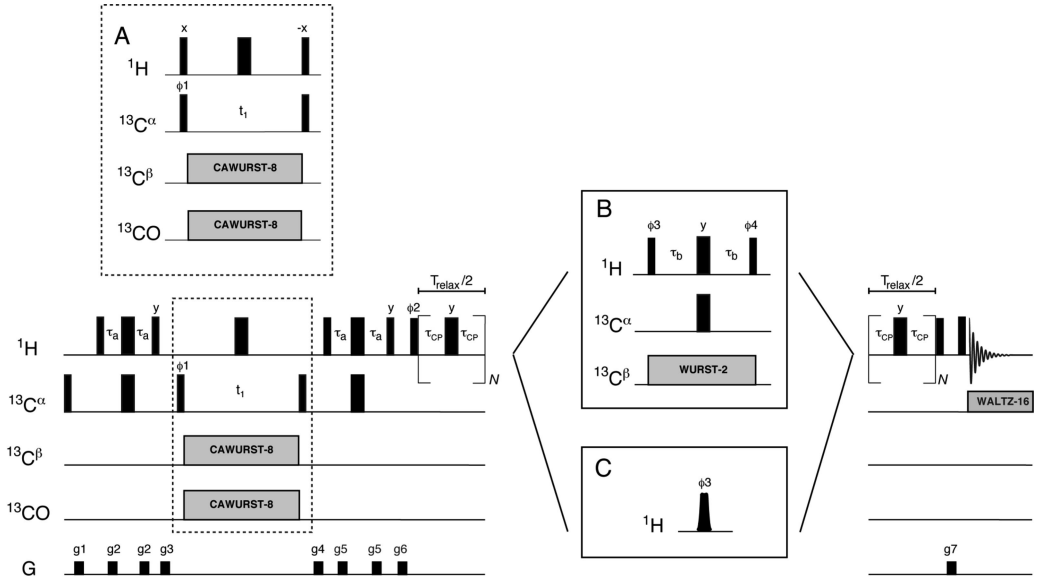

Figure 2. Pulse scheme of the $^1H^\alpha$ CPMG relaxation dispersion experiment for measuring millisecond time-scale dynamics in uniformly ^{13}C-labeled, fractionally deuterated proteins. ^1H and ^{13}C 90° (180°) RF pulses are shown as narrow (wide) bars. The ^1H carrier is placed on the water signal, while the ^{13}C carrier is at 58 ppm. All pulse phases are assumed to be x, unless indicated otherwise. ^1H and ^{13}C pulses are applied at the highest possible power level, except for the ^1H pulses applied immediately after gradient g6 and prior to gradient g7 which use a field strength of approximately 25 kHz. ^{13}CO and $^{13}C^\beta$ spins are decoupled during the $^{13}C^\alpha$ evolution period using simultaneous decoupling fields comprised of constant adiabicity WURST-8 schemes.[59,60] For ^{13}CO decoupling the field is centered at 175 ppm, decoupling bandwidth = 10 ppm and max(rms) field strength of 0.39(0.29)kHz, while for $^{13}C^\beta$ decoupling a field was applied with a decoupling bandwidth of 30 ppm and max(rms) field strengths of 0.49(0.39)kHz, swept from 15 to 45 ppm (centered at 30 ppm). An additional equivalent field swept from 110 to 71 ppm (centered at 86 ppm) was applied as well that essentially eliminates decoupling artifacts that would otherwise manifest when only a single field centered at 30 ppm is applied.[60,61] A 180° ^{15}N pulse, centered at 119 ppm, is applied in the middle of the t_1 period in the case of samples that are also ^{15}N labeled. To increase sensitivity in larger proteins, multiple-quantum evolution in t_1 can be employed by substituting the element shown in inset (A) for the block within the dashed box in the main figure. ^{13}C decoupling during acquisition is achieved with a 2.5 kHz WALTZ-16 scheme.[62] The phase cycling used is: $\phi_1 = x, -x, \phi_2 = 2(x), 2(-x), \phi_3 = 4(x), 4(-x), \phi_4 = 4(-x), 4(x)$, receiver $= x, -x, -x, x$. The delay τ_a is set to 1.8 ms and N is any even number. Gradient strengths G/cm (length in ms) are: $g_1 = 5.0(1.0)$, $g_2 = 8.0(0.6)$, $g_3 = -12.0(1.0)$, $g_4 = 15.0(0.3)$, $g_5 = -8.0(0.1)$, $g_6 = 8.0(0.5)$, $g_7 = 15.0(0.4)$. Quadrature detection in the indirect dimension is obtained by recording two sets of spectra with (ϕ_1) and ($\phi_1 + \pi/2$) for each t_1 increment;[63] the phase ϕ_1 and the receiver are incremented by 180° for each complex t_1 point.[64] The insets (B) and (C) show refocusing elements that partially suppress the effects of $^3J_{H\alpha,H\beta}$ couplings. (B) Delay $\tau_b = 1/(2^1J_{H\alpha,C\alpha})$ is set to 3.52 ms. $^{13}C^\beta$ decoupling is achieved with a WURST-2 scheme[65] centered at 27.5 ppm and with a bandwidth of 25 ppm, max(rms) field strength of 1.22(0.69) kHz. The $^{13}C^\beta$ spins of Thr and Ser are not decoupled using this scheme and these residues are therefore unavailable for analysis. The shaped pulse in (C) refocuses $^1H^\alpha$ (code for generating this pulse is available on request). In the present application it was centered at 4.77 ppm and applied with a width of 1.65 ms at 800 MHz (scaled appropriately for the other fields). The pulse gives at least 96% inversion from 3.3 to 6.24 ppm and less than 1% inversion upfield of 2.0 ppm.

magnetization intensity will depend on τ_{CP}, even in the absence of chemical exchange, leading to dispersion profiles that are not flat and complicating the extraction of accurate exchange parameters when exchange is present. Of course, the situation is more complex than what is reported by eqs 1 and 2 since in general (1) refocusing pulses are not perfect, (2) relaxation cannot be neglected and (3) the network of scalar coupled proton spins will be larger than that considered here.

Removing Homonuclear Scalar Couplings via Deuteration. Ideally one would like to generate protein samples with full protonation at the C^α position that are completely deuterated at all other sites. Very close to ideal would be to produce samples that at a minimum are highly deuterated at the C^β carbon since then the problematic $^1H^\alpha$-$^1H^\beta$ scalar couplings would be eliminated. The simultaneous goal of generating proteins with high levels of protonation at the C^α position while C^β is deuterated for proteins produced with traditional overexpression protocols that use glucose as the carbon source in M9 medium is not achieved easily since, regrettably, H^α and to some extent H^β derive from a common source—solvent. However, since the H^β protons for most of the residues also, at least in part, originate from glucose (while the protonation content at the α-position is derived from solvent[52]) the use of deuterated glucose will lead to fractional deuteration at C^β but not at C^α. To further increase the level of deuteration at C^β it is possible perform overexpression in a mixture of D_2O and H_2O, although at the expense of partial deuteration at the α-position. The optimal fraction of D_2O is thus necessarily a compromise between having the C^α position highly protonated to maximize sensitivity while maintaining a high level of deuteration at C^β to avoid artifacts. Here we have settled for protein expression in 50% D_2O/50% H_2O using perdeuterated ^{13}C glucose that, as we show below, achieves levels of deuteration at the C^β position that range between 50 and 88%, depending on residue type.

The residue-specific pattern of deuteration that is achieved at C^β using the precursors described above can be understood by noting that amino acids are synthesized from intermediates of a small set of metabolic pathways, including glycolysis, the tricarboxylic acid (TCA) cycle and the pentose phosphate pathway[52] and by following the levels of protonation of the various precursors along these pathways. The predicted isotopomer composition at the β-position for the glycolytic amino acids, using uniformly deuterated glucose and 50% D_2O is described in Figure 1A, with the level of deuterium incorporation at each of the two positions in 3-phosphoglycerate independent of the other, see below. The first important step along the pathway is the isomerization of glucose-6-phosphate (G6P) to fructose-6-phosphate (F6P) during which a hydrogen is transferred from position 2 to 1.[56] In theory, position 1 of fructose-6-phosphate should thus be uniformly deuterated but since the deuteron is transiently located on a catalytic His residue of the

enzyme that catalyzes this reaction it may exchange with solvent. Here we consider the worst-case scenario where the deuteron is exchanged for a proton, resulting in 50% CD_2, 50% CDH at position 1 of F6P. F6P is subsequently phosphorylated at position 1 to yield fructose-1,6-bisphosphate (FBP) that undergoes a series of reactions to produce 3-phosphoglycerate (3PG) and then phosphoenolpyruvate (PEP), with the isotopomer composition shown in the figure. Since these molecules are the precursors for Cys, Phe, Ser, Trp, and Tyr, with position 3 corresponding to C^β for these amino acids, the isotopomer composition at this position will be 75% CD_2, 25% CDH. In the last step of glycolysis, PEP is dephosphorylated and picks up a hydrogen atom from solvent to yield pyruvate, the precursor of Ala. Position 3 of pyruvate corresponds to C^β of Ala, leading to an isotopomer composition of 37.5% CD_3, 50% CD_2H, 12.5% CDH_2 for this residue. Lys, for which the β-position may also be derived from position 3 of pyruvate, is produced with an isotopomer distribution of 54% CD_2, 42% CDH, 4% CH_2 that readily follows after abstraction of a hydrogen (H or D) from the methyl position.

The origin of the isotopomer composition at the β-position for the amino acids derived from TCA cycle intermediates can be understood from Figure 1B. Here the level of deuteration at a given position is indicated as in Figure 1A, with the extent of incorporation of label at one site in a precursor molecule independent from another. Thus, in the case of citrate there are 9 different labeling possibilities with, for example, a probability of 0.75*0.54 for CD_2 at both positions 2 and 4. In the first step of the TCA cycle oxaloacetate (OA) and acetyl-S-CoA (Ac−S−CoA) condense to yield citrate and through a series of reactions OA is regenerated at the end of the cycle. The precursor of Arg, Gln, Glu and Pro, α-ketoglutarate (AKG), is formed in four steps by decarboxylation of citrate accompanied by oxidation at position 2 and reduction at position 3. Both hydrogen atoms at position 3 of AKG, which is the "source" of C^β for the above amino acids, are derived from solvent, leading to a β-position isotopomer composition for Arg, Gln, Glu and Pro of 25% CD_2, 50% CDH and 25% CH_2. AKG is then decarboxylated, oxidized, and dehydrogenated in three steps to yield fumarate that has a deuteration pattern that can be readily calculated from the isotopomer distribution in AKG. Because of the symmetry of fumarate, a given molecule of malate will have an isotopomer composition at position 3 that depends on the carbon in fumarate from which it is derived; summing over all possibilities gives the distribution listed (31% CD_2, 50% CDH, 19% CH_2). Finally OA that is formed in the last step of the TCA cycle preserves the isotopomer distribution of its precursor malate. As indicated in the figure, OA can also be synthesized by carboxylation of PEP and in this case its isotopomer composition at position 3 is 75% CD_2, 25% CDH. The overall level of deuteration of OA depends, therefore, on the relative rates of carboxylation of PEP and oxidation of malate. On the basis of earlier studies,[57] we estimate that 30% of OA is formed by carboxylation of PEP, 70% from oxidation of malate (note that this is dependent on growth conditions) and predict that the net isotopomer composition at position 3 of OA and thus also at the β-position of its derived amino acids Asn, Asp and Met will be 44% CD_2, 43% CDH and 13% CH_2. Note that the level of deuteration at the β-position of Thr can be easily established since it is derived from Asp. The β-position of Lys is equally likely to be derived from position 3 of OA or position 3 of pyruvate because these two precursors form a symmetric intermediate in its biosynthesis, L,L-α,ε-diaminopimelate.[52] The C^β isotopomer composition of Lys is thus given by the average of the distribution found at position 3 of both OA and pyruvate (in the latter case after first removing one hydrogen atom). It is noteworthy that both hydrogen atoms at position 3 of OA are lost in one round of the TCA cycle, so that the level of deuterium incorporation at the C^β position of amino acids is independent of the number of passes that their precursors make through the cycle.

His is synthesized from the pentose phosphate pathway intermediate ribose-5-phosphate, and its β-position is ultimately derived from deuterated C4 of glucose. An additional hydrogen atom is picked up from solvent so that the isotopomer composition at the β-position of this residue is 50% CD_2, 50% CDH. The β-hydrogens of all the remaining amino acids, Ile, Leu and Val are derived from solvent, resulting in an isotopomer composition of 50% CD, 50% CH (Ile, Val) and 25% CD_2, 50% CDH, 25% CH_2 (Leu). The predicted isotopomer composition as well as the overall deuteration level at the β-position for each of the amino acids is summarized in Table 1, where amino acids with the same isotopomer pattern are grouped together.

Table 1. Predicted Isotopomer Composition and Overall Deuteration Level at the β-Positions in a Protein Expressed with Uniformly Deuterated Glucose as the Carbon Source in 50% D_2O/50% H_2O

amino acid	$CD_3/CD_2/CD$[a]	$CD_2H/CDH/CH$	CDH_2/CH_2	overall deuteration
Cys, Phe, Ser, Trp, Tyr	0.75	0.25		0.88
Arg, Gln, Glu, Leu, Pro	0.25	0.50	0.25	0.50
Asn, Asp, Met	0.44	0.43	0.13	0.66
Ile, Val	0.50	0.50		0.50
Ala	0.37	0.50	0.13	0.75
His	0.50	0.50		0.75
Lys	0.49	0.42	0.09	0.70
Thr	0.66	0.34		0.66

[a] The most deuterated isotopomer is reported in column 1, the second most deuterated in column 2 and so forth, regardless of whether this refers to groups with one, two or three hydrogen atoms. For example, for the amino acids Cys, Phe, Ser, Trp or Tyr, the relevant column headers would be CD_2, CHD and CH_2, whereas for Ala they are CD_3, CD_2H, CH_2D.

Table 2. Predicted and Measured Fraction of the Fully Protonated C^β Isotopomer in Samples Prepared with Uniformly Deuterated Glucose as the Carbon Source, 50% D_2O/50% H_2O

residue	predicted	measured[a]
Ala	0.00	0.05 ± 0.03 (3)
Asn	0.13	0.11 ± 0.04 (7)
Asp	0.13	0.14 ± 0.04 (6)
Arg	0.25	n.a.[b]
Cys	0.00	n.a.[b]
Gln	0.25	n.a.[b]
Glu	0.25	0.23 ± 0.02 (7)
His	0.00	n.a.[b]
Ile	0.50	0.55 ± 0.05 (3)
Leu	0.25	0.28 ± 0.03 (4)
Lys	0.09	0.16 ± 0.02 (4)
Met	0.13	0.12 (1)
Phe	0.00	n.a.[c]
Pro	0.25	0.18 ± 0.06 (4)
Ser	0.00	0.04 ± 0.002 (3)
Thr	0.34	0.39 ± 0.002 (2)
Trp	0.00	n.a.[c]
Tyr	0.00	n.a.[c]
Val	0.50	0.57 ± 0.02 (3)

[a] Results from quantification of spectra recorded on the Abp1p SH3 domain. [b] These amino acids are not present in Abp1p SH3 domain. [c] The peak corresponding to the fully protonated isotopomer could not be detected.

The predicted isotopomer distribution can be verified to some extent in a straightforward manner by analyzing $^{13}C-^{1}H$ correlation spectra recorded on samples that have been prepared using $U-^{13}C$, ^{2}H glucose and 50% D_2O/50% H_2O. Here we have compared intensities of peaks derived from $^{13}C^{\beta}H^{\beta}_2$ moieties ($^{13}C^{\beta}H^{\beta}$ in the case of Ile, Thr and Val, and $^{13}C^{\beta}H^{\beta}_3$ for Ala) in a labeled sample of an Abp1p SH3 domain prepared in this manner with intensities measured in a spectrum of a fully protonated, ^{13}C labeled sample. Differences in sample concentrations were accounted for by normalization of spectra to the average ratio of the intensities of $^{13}C^{\alpha}-^{1}H^{\alpha}$ correlations in each spectrum, taking into account that for equal protein concentrations only 1/2 the intensity should be observed in spectra of the sample prepared with 50% D_2O. Table 2 lists the predicted and measured fractions of fully protonated C^{β} isotopomers for each amino acid and in general there is excellent agreement. Quantification was possible for all residue types in the Abp1p SH3 domain except Phe, Trp and Tyr, where the $^{13}C^{\beta}H^{\beta}_2$ isotopomer is not expected, and where cross-peaks corresponding to $^{13}C^{\beta}H^{\beta}_2$ could not be detected. A small but significant fraction of fully protonated C^{β} has been measured for Ala, that results from exchange of the acidic methyl protons of pyruvate with solvent and accordingly the experimental measurements for Lys do not agree completely with predictions. In principle, it is possible to extend this analysis to include a comparison of the relative ratios of $^{13}C^{\beta}H^{\beta}_2$ and $^{13}C^{\beta}H^{\beta}D^{\beta}$ isotopomers. However, the different relaxation properties of magnetization derived from each of these spin systems would have to be properly taken into account before accurate quantification could be made, especially considering that constant-time spectra are recorded with relatively long fixed delays during which signal decay occurs. We have chosen not to pursue this, given the close agreement between prediction and experiment that is established on the basis of the CH_2 data shown in Table 2 that supports the accuracy of the predictions listed in Table 1 in general.

Suppressing the Effects of Residual Homonuclear Scalar Couplings by Experiment. The high levels of deuteration that have been achieved using the labeling scheme described above prompted us to evaluate whether a simple CPMG pulse sequence using nonselective proton refocusing pulses alone would be sufficient to obtain robust $^{1}H^{\alpha}$ dispersion profiles. Unfortunately, despite the fact that the effects of $^{1}H^{\alpha}-^{1}H^{\beta}$ scalar couplings are significantly attenuated in samples prepared using $^{2}H-$glucose and 50% H_2O/50% D_2O relative to fully protonated proteins, they are not completely eliminated and dispersion profiles were obtained that were not of sufficient quality to be useful. A pair of pulse schemes, Figure 2B,C, have therefore been developed that are distinct alternatives for the suppression of the effects of the remaining scalar couplings (in what follows the utility of scheme B will be discussed first). The basic flow of magnetization of interest during these sequences can be described as

$$^{1}H^{\alpha}\rightarrow{}^{13}C^{\alpha}(t_1)\rightarrow{}^{1}H^{\alpha}\rightarrow \mathrm{CPMG}\rightarrow{}^{1}H^{\alpha}(t_2) \qquad (3)$$

and a series of $^{13}C-^{1}H$ correlation maps are obtained that vary only in ν_{CPMG}. It is possible to record ^{13}C chemical shifts in either single- (main Figure) or multiple-quantum ($^{1}H^{\alpha}-^{13}C^{\alpha}$) mode[58] (scheme A). In the present study involving a relatively small protein system (≈7 kDa) we record spectra with single-quantum acquisition in t_1, although higher gains in sensitivity will be achieved for larger proteins when the coherences of interest are multiple-quantum during t_1, especially since there is a high level of deuterium incorporation at the β-position for most residues in the samples used here. Indeed, in a recent application involving a T4 lysozyme mutant (correlation time of approximately 11 ns) we have noted sensitivity gains of a factor of 1.2 ± 0.1 in favor of the multiple-quantum spectra (based on quantification of 40 well resolved correlations), with only one residue showing a decrease in intensity.

As described above the application of successive ^{1}H refocusing pulses during the CPMG period modulates the evolution of $^{1}H^{\alpha}$ magnetization due to $^{1}H^{\alpha}$-$^{1}H^{\beta}$ couplings in a manner dependent on ν_{CPMG}, that severely compromises the utility of the resulting dispersion profiles (see eqs 1 and 2). With this in mind we have modified the constant time CPMG interval by inserting a *J*-refocusing element in the middle (inset B in Figure 2) that refocuses scalar coupled evolution of a two-spin coupled $^{1}H^{\alpha}-^{1}H^{\beta}$ spin pair in the limit that pulse imperfections and relaxation are neglected. It is worth noting that while the $^{1}H^{\alpha}-^{1}H^{\beta}$ two-spin system considered is an oversimplification in the context of a fully protonated protein where side-chains are comprised of a highly coupled proton network, the high levels of deuteration achieved using the present labeling scheme means that such an approximation is much more reasonable for the labeled proteins studied here.

Our design of the *J*-refocusing element of Figure 2B was based on an analysis that considers the evolution of a two spin $^{1}H^{\alpha}-^{1}H^{\beta}$ spin system, neglecting relaxation and pulse imperfections during the CPMG element. Under this set of conditions and starting from I_Y^{α}, the magnetization of interest at the midpoint of the CPMG element, $T_{relax}/2$, is given by

$$I_Y^{\alpha}\cos\left(\pi J_{\alpha\beta}\frac{T_{relax}}{2}\right)-2I_X^{\alpha}I_Z^{\beta}\sin\left(\pi J_{\alpha\beta}\frac{T_{relax}}{2}\right)$$

and by

$$I_Y^{\alpha}\cos^2\left(\pi J_{\alpha\beta}\frac{T_{relax}}{2}\right)+I_Y^{\beta}\sin^2\left(\pi J_{\alpha\beta}\frac{T_{relax}}{2}\right)+(I_Z^{\alpha}I_X^{\beta}-I_X^{\alpha}I_Z^{\beta})\sin(\pi J_{\alpha\beta}T_{relax}) \qquad (4)$$

in the limiting cases of very slow and very rapid pulsing, respectively. Application of the ^{1}H $90°_{\phi3}$ pulse at the start of the *J*-refocusing element places Y-magnetization along the Z-axis so that for $J_{\alpha\beta}\approx 0$ all of the magnetization of interest is longitudinal and relaxation losses during this interval are minimized. In contrast, the ^{1}H $90°_{\phi3}$ converts antiphase transverse magnetization that accumulates during the first half of the CPMG pulse train for $J_{\alpha\beta}\neq 0$ (denoted by terms $2I_X^{\alpha}I_Z^{\beta}$,$(I_Z^{\alpha}I_X^{\beta}-I_X^{\alpha}I_Z^{\beta})$ of eq 4) into linear combinations of double- and zero-quantum coherences ($2I_Y^{\alpha}I_X^{\beta}$,$2I_X^{\alpha}I_Y^{\beta}$). During the subsequent delay of duration $1/J_{H\alpha C\alpha}$ evolution proceeds due to $^{1}H^{\alpha}-^{13}C^{\alpha}$ couplings while the band-selective $^{13}C^{\beta}$ decoupling that is applied ensures that evolution from $J_{H\beta C\beta}$ does not occur. In this way the multiple-quantum coherences are inverted in sign and immediately following the refocusing element the magnetization of interest is

$$-I_Y^{\alpha}\cos\left(\pi J_{\alpha\beta}\frac{T_{relax}}{2}\right)-2I_X^{\alpha}I_Z^{\beta}\sin\left(\pi J_{\alpha\beta}\frac{T_{relax}}{2}\right)$$

and

$$-I_Y^{\alpha}\cos^2\left(\pi J_{\alpha\beta}\frac{T_{relax}}{2}\right)-I_Y^{\beta}\sin^2\left(\pi J_{\alpha\beta}\frac{T_{relax}}{2}\right)+(I_Z^{\alpha}I_X^{\beta}-I_X^{\alpha}I_Z^{\beta})\sin(\pi J_{\alpha\beta}T_{relax}) \qquad (5)$$

It can be shown that evolution during the second half of the CPMG interval leads to complete refocusing of the effects of $^{1}H^{\alpha}-^{1}H^{\beta}$ scalar couplings so that the term of interest at the end of the CPMG pulse train is $-I_Y^{\alpha}$. Simulations (that again neglect pulse imperfections) have also established that refocusing is very efficient not only in the limiting cases that are readily considered

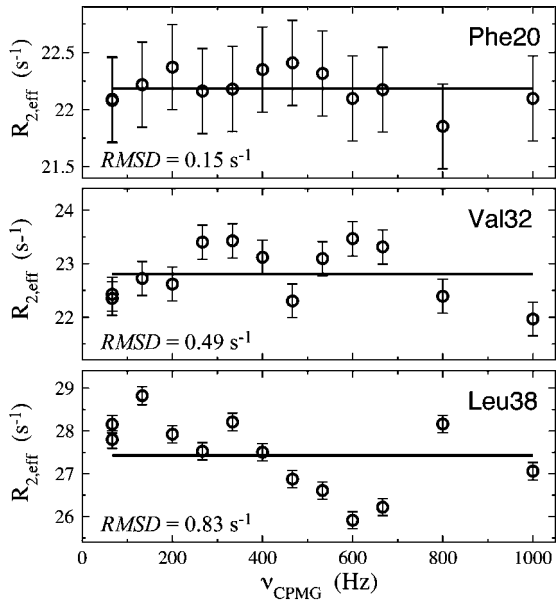

Figure 3. $^1H^\alpha$ dispersion profiles for residues Phe20, Val32 and Leu38 recorded on a fractionally deuterated, uniformly ^{13}C labeled apo Abp1p SH3 domain sample at 25 °C using the pulse sequence in Figure 2B that includes the *J*-refocusing element. Symbols indicate data recorded at 600 MHz and the corresponding lines result from fits to a model where $R_{2,\text{eff}}$ = constant. The panels show (top to bottom) examples of residues with low, average and high rmsd between experiment and model.

analytically but over the complete range of $\Delta\omega\tau_{CP}$, resulting in flat dispersion profiles in the absence of chemical exchange. In addition to refocusing $^1H^\alpha-^1H^\beta$ scalar couplings there is another advantage in using the scheme of Figure 2B. The refocusing pulses during the CPMG train are of course not perfect and imperfections lead to the creation of small amounts of X- and Z-components of magnetization, in addition to the desired Y-component. The *J*-refocusing scheme employed inverts both the Y- and Z-magnetization components, but not the X, and it has been shown previously that this leads to a complete refocusing of the effects of pulse imperfections at the end of the CPMG period,[35,66] at least in applications involving spin systems for which homonuclear couplings are negligibly small (for example for ^{15}N relaxation dispersion studies). Simulations establish that the combination of homonuclear couplings and pulse imperfections during the CPMG train results in magnetization evolution that is more complex than that indicated by eqs 4 and 5, reducing the efficacy of the *J*-refocusing scheme somewhat. Further, relaxation during the refocusing element can also decrease its efficiency. As we will show below, however, for the labeling scheme used here that significantly decreases the level of protonation at the C^β position the methodology is still efficient.

Experimental Verification. As a first step to verify the robustness of the pulse scheme of Figure 2 with the *J*-refocusing element (Figure 2B) we have recorded $^1H^\alpha$ dispersion profiles on an SH3 domain from the yeast protein Abp1p.[46−48] In the absence of added peptide (see below) exchange is not expected and flat dispersion profiles are therefore anticipated. Indeed this is what is obtained as Figure 3 illustrates for a number of profiles, where the pair wise rmsd between each curve and the best-fit horizontal line is indicated. We have chosen the 3 residues in the figure because they are among those with the lowest (0.15 s^{-1}), average (0.49 s^{-1}) and highest (0.83 s^{-1}) rmsd values. The high rmsd for Leu 38 (Figure 3) reflects the incomplete deuteration at the C^β position of Leu residues that is obtained using our scheme (Table 1) and the fact that there is incomplete refocusing of evolution from the $^1H^\alpha-^1H^\beta$ scalar coupling because of the downfield C^β shift of this residue (46.5 ppm, see below). An average rmsd of 0.52 ± 0.35 s^{-1} based on analysis of dispersion data from 56 residues was obtained that decreases to 0.48 ± 0.22 s^{-1} (51 residues) when Ser and Thr are omitted (see below).

As a second step we sought to establish that accurate values of $^1H^\alpha$ chemical shift differences can be extracted from fits of relaxation dispersion data. Here we have used the exchanging system described previously,

$$P + L \underset{k_{off}}{\overset{k_{on}}{\rightleftharpoons}} PL, \quad K_D = 0.55 \pm 0.05\ \mu M \tag{6}$$

where *P* and *L* correspond to the Abp1p SH3 domain (described above) and a 17 residue binding peptide from the protein Ark1p,[49] respectively. The addition of only a small mole fraction of *L* (≈5%) ensures that *P* remains the visible, ground-state whose resonances are observed in NMR spectra while the bound conformation, *PL*, that is populated to only approximately 5%, becomes the invisible, excited state. Under these conditions and at 25 °C the exchange rate, $k_{ex} = k_{on}[L] + k_{off}$, is several hundreds/sec, so that the exchange reaction can be well quantified by the CPMG technique. The chemical shift differences between *P* and *PL* that are measured from CPMG experiments can subsequently be compared to those obtained directly from measurements on samples comprising only *P* (no *L*) or *PL* (saturating amounts of *L*) and in this manner the accuracy of the chemical shifts of the excited-state can be quantified.

The Ark1p peptide was titrated into a sample of the apo SH3 domain to an estimated mole fraction of 5% based on analysis of ^{15}N relaxation dispersion data and this sample was used to record $^1H^\alpha$ dispersions using the pulse sequence described in Figure 2B that makes use of the *J*-refocusing element described above. Representative $^1H^\alpha$ dispersion profiles are shown in Figure 4 for a number of residues in the SH3 domain. Dispersion curves for 19 residues recorded at static magnetic fields corresponding to ^1H resonance frequencies of 600 and 800 MHz have been fit to a model of two-site chemical exchange (see Materials and Methods) and chemical shift differences, $|\Delta\varpi_{CPMG}|$, extracted. It is well-known that relaxation dispersion experiments are insensitive to the signs of the shift differences.[13] In principle, these can be obtained from knowledge of the relative signs of $\Delta\varpi(^1H^\alpha)$ and $\Delta\varpi(^{13}C^\alpha)$ that are available from a comparison of $^1H^\alpha-^{13}C^\alpha$ double- and zero-quantum dispersion profiles[67,68] once the sign of $\Delta\varpi(^{13}C^\alpha)$ is known.[34] These experiments are beyond the scope of the present paper, however, and here we report $|\Delta\varpi|$. Values of $|\Delta\varpi_{CPMG}|$ are compared with those measured directly from peak positions in free and fully bound samples, $|\Delta\varpi_{Direct}|$, in Figure 5. A pairwise rmsd of 0.032 ppm is obtained between $|\Delta\varpi_{CPMG}|$ and $|\Delta\varpi_{Direct}|$ based on the 19 residues for which $\Delta\varpi$ values could be extracted (determined by F-test analyses described in Materials and Methods), with the largest deviation being 0.09 ppm for Ile26. Errors of this order are well under the limits of accuracy of the best available prediction algorithms, approximately 0.3 ppm.[42]

(66) Hansen, D. F.; Vallurupalli, P.; Kay, L. E. *J. Phys. Chem. B* **2008**, *112*, 5898–5904.
(67) Korzhnev, D. M.; Neudecker, P.; Mittermaier, A.; Orekhov, V. Y.; Kay, L. E. *J. Am. Chem. Soc.* **2005**, *127*, 15602–15611.
(68) Kloiber, K.; Konrat, R. *J. Biomol. NMR* **2000**, *18*, 33–42.

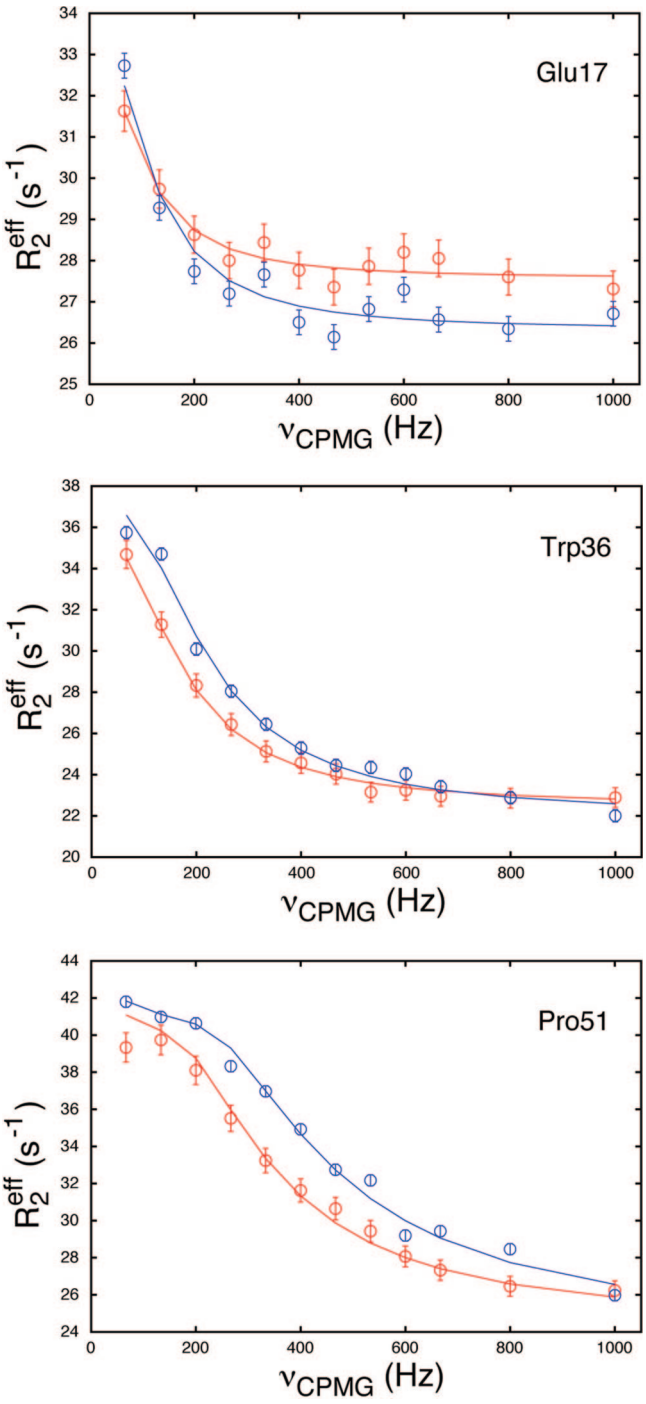

Figure 4. $^1H^\alpha$ dispersion profiles for residues Glu17, Trp36 and Pro51 recorded on a fractionally deuterated, uniformly ^{13}C labeled Abp1p SH3 domain sample with ~5% bound peptide at 25 °C using the pulse sequence in Figure 2B that includes the *J*-refocusing element. Blue (red) symbols indicate data recorded at 800 (600) MHz and the corresponding lines result from fits to a two-state exchange model.

It must be emphasized that flat dispersions also provide useful information since they establish that the chemical shifts for the ground and excited states are equivalent. In Figure 5B we have plotted the correlation between $|\Delta\varpi_{CPMG}|$ (black) and $|\Delta\varpi_{Direct}|$ (red) as a function of residue number; black bars are not included for residues for which flat dispersion profiles are obtained or for Gly, Ser and Thr (see below). It is obvious that the set of residues for which flat profiles are obtained overlaps well with the set of residues with small

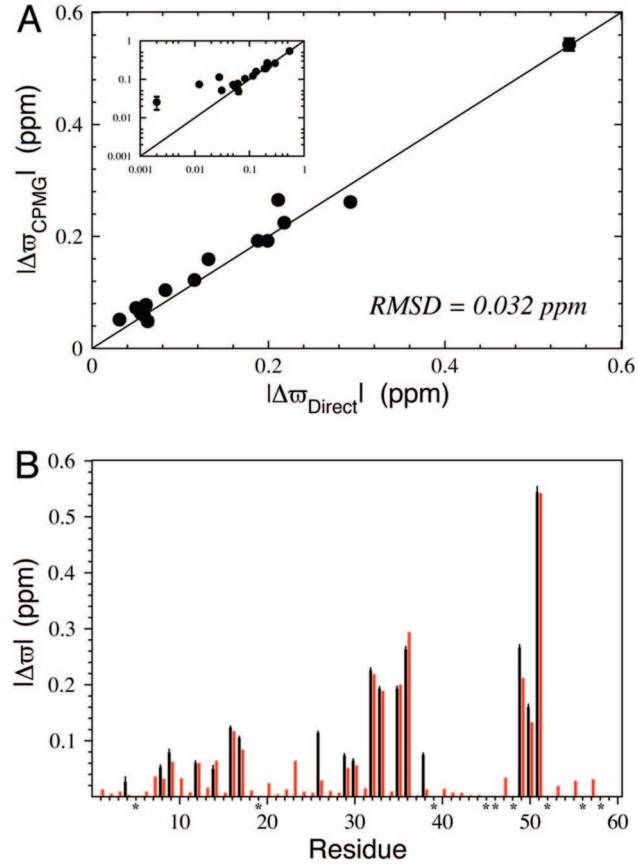

Figure 5. (A) Correlation between $^1H^\alpha$ $|\Delta\varpi|$ values (ppm) extracted from fits of relaxation dispersion data recorded on a fractionally deuterated, uniformly ^{13}C labeled Abp1p SH3 domain sample (~5% peptide) using the pulse sequence of Figure 2B that includes the *J*-refocusing element (*y* axis) and the corresponding values measured directly from samples of free and fully bound Abp1p SH3 domains (*x* axis). The solid line ($y = x$) corresponds to a perfect correlation between the two data sets. Only points for which $|\Delta\varpi| > 0.02$ ppm are retained in the main figure while all data points are shown in the inset as a log/log plot. The rmsd between the two data sets is indicated in the figure. (B) $^1H^\alpha$ $|\Delta\varpi|$ values extracted from relaxation dispersion data (black) or based on direct measurements in free and fully bound SH3 domains (red) plotted vs. residue number. Residues for which it was not feasible to measure dispersions, that is, Gly, Ser and Thr (see text), are marked with an asterisk. Other gaps in the plot imply that the chemical shifts are the same in the free and bound states of the Abp1p SH3 domain.

values of $|\Delta\varpi_{Direct}|$. In no case did we fail to identify chemical exchange for a residue with $|\Delta\varpi_{Direct}| > 0.1$ ppm and in only one case for $|\Delta\varpi_{Direct}| > 0.05$ ppm (Asn23). The two largest outliers in the figure are Ile26 and Leu38 where ($|\Delta\varpi_{CPMG}|$, $|\Delta\varpi_{Direct}|$) = (0.11,0.03)ppm and (0.07,0.01)ppm, respectively, and notably the dispersion profiles for these residues did not resemble those obtained for others; rather they suggested a faster exchange process. The small errors in chemical shifts for these residues can be explained by incomplete decoupling of $^{13}C^\beta$ during the *J*-refocusing element, leading to incomplete refocusing of residual $^1H^\alpha-^1H^\beta$ scalar couplings, since the $^{13}C^\beta$ chemical shifts for Ile26 and Leu38 are 40.6 and 46.5 ppm, respectively, and the $^{13}C^\beta$ decoupling range extends from 15 to 40 ppm. This also explains why the deviation between $|\Delta\varpi_{CPMG}|$ and $|\Delta\varpi_{Direct}|$ for Leu 49 is among the largest observed (0.06 ppm) since its $^{13}C^\beta$ chemical shift is 45.7 ppm. If these three residues are removed the rmsd between $|\Delta\varpi_{CPMG}|$ and $|\Delta\varpi_{Direct}|$ drops to 0.018 ppm, very close to what was obtained for $^1H^N$ in a previous study.[34]

The fact that artifacts are seen for these residues but not for others with $^{13}C^{\beta}$ carbons resonating downfield of 40 ppm is likely due to the fact that they are only deuterated to 50% at $^{13}C^{\beta}$ (see Table 1 for Ile, Leu), emphasizing the importance of deuteration in these experiments. Finally, it is worth noting that profiles from Ser and Thr were excluded from analysis since $^{13}C^{\beta}$ chemical shifts are far downfield of the decoupling range used in the *J*-refocusing element.

It is very clear from the above discussion that the application of the dispersion experiment of Figure 2B with the *J*-refocusing element to samples prepared with U−^{2}H glucose and 50% D_2O/50% H_2O allows the measurement of robust $^{1}H^{\alpha}$ dispersion profiles, leading to the accurate extraction of chemical shift differences. However, neither the labeling, nor the refocusing is "perfect". It is of interest, therefore, to consider an alternative approach (with perhaps somewhat different limitations) and to compare $|\Delta\varpi_{CPMG}|$ from both methods. Figure 2C illustrates a second pulse scheme with the *J*-refocusing element of Figure 2B replaced by a $^{1}H^{\alpha}$ band-selective refocusing pulse. Ishima and Torchia have also proposed using a band selective pulse to refocus evolution due to homonuclear scalar couplings in ^{1}HN CPMG studies of protonated proteins.[54] In the present case, so long as magnetization from $^{1}H^{\alpha}$ but not $^{1}H^{\beta}$ is effected by the pulse, evolution from residual $^{1}H^{\alpha}-^{1}H^{\beta}$ scalar couplings will be refocused in the weak pulsing limit. Refocusing does not occur outside this limit, even in the absence of pulse imperfections during the CPMG pulse train, however, since the finite duration of the $^{1}H^{\alpha}$ band-selective pulse leads to evolution of transverse $^{1}H^{\beta}$ magnetization (see eq 2). Nevertheless, for shift differences >2 ppm, applications at 800 MHz and $\nu_{CPMG} < 1$ kHz it follows that $|\Delta\omega\tau_{CP}| \geq 2.5$ so that the weak pulsing limit is operative and one might expect, therefore, that largely artifact free dispersion profiles would be obtained with this approach as well. Figure 6 shows that this is indeed the case, with a pairwise rmsd of 0.022 ppm obtained in a comparison of $|\Delta\varpi|$ values extracted from relaxation dispersion profiles and from direct chemical shift measurements of free and fully bound SH3 domains. Discrepancies between $|\Delta\varpi_{CPMG}|$ and $|\Delta\varpi_{Direct}|$ are not noted in cases where the chemical shifts of $^{1}H^{\beta}$ are such that β-proton magnetization is not perturbed by the $^{1}H^{\alpha}$ "selective" pulse (shifts upfield of 2.0 ppm).

Both schemes of Figure 2 are effective, at least in the present case, but we prefer the *J*-refocusing method for a number of reasons. First, it is not feasible to pulse on $^{1}H^{\alpha}$ without affecting $^{1}H^{\beta}$ magnetization for at least some of the residues in a protein. This is a particular concern for residues in α-helices relative to β-strands since the chemical shifts of $^{1}H^{\alpha}$ are shifted upfield in α-helices, and although $^{1}H^{\beta}$ chemical shifts are less sensitive to backbone conformation, they are on average displaced downfield by 0.04 ppm.[69] By contrast, the *J*-refocusing strategy is expected to perform better for α-helical proteins since the chemical shifts of $^{13}C^{\alpha}$ and $^{13}C^{\beta}$ are better separated than in their β-sheet counterparts,[40] so that $^{13}C^{\beta}$ decoupling should be more effective for a larger number of residues. The two methods thus complement each other. A second advantage of the *J*-refocusing element is that its efficacy is independent of the pulse rate, $\Delta\omega\tau_{CP}$, at least in the absence of pulse imperfections during the CPMG train, unlike the case for the method involving the selective $^{1}H^{\alpha}$ pulse. Finally, it should be noted that there are some residue types for which neither method performs well. For example, the two $^{1}H^{\alpha}$ protons of Gly are problematic and we are in the process of developing a Gly-specific experiment. The $^{13}C^{\alpha}$ and $^{13}C^{\beta}$ carbons of Ser usually resonate in the same region so that the *J*-refocusing strategy is not an option. Unfortunately, $^{1}H^{\alpha}$ and $^{1}H^{\beta}$ chemical shifts of Ser are in general similar so that refocusing using the $^{1}H^{\alpha}$ selective pulse also usually fails. Of interest, the $^{1}H^{\alpha}$ and $^{1}H^{\beta}$ chemical shifts for Ser52 are 2.71 and 1.34/1.76 ppm respectively so that the selective $^{1}H^{\alpha}$ refocusing pulse does not perturb the $^{1}H^{\beta}$ spins in this unusual case. In general, similar problems hold for Thr as well. For Ser and Thr it may be preferable to use $^{13}C^{\alpha}$ selectively labeled samples so that the *J*-refocusing element can be performed in the absence of $^{13}C^{\beta}$ decoupling. $^{13}C^{\alpha}$ selective labeling for these residue types can be accomplished by using [2-^{13}C]-glucose as the carbon source during overexpression, leading to 45% and 30% ^{13}C enrichment at the C^{α} position for Ser and Thr, respectively.[70] Alternatively, [2-^{13}C]-glycerol[71] or [2-^{13}C]-pyruvate can be used. These carbon sources effectively double

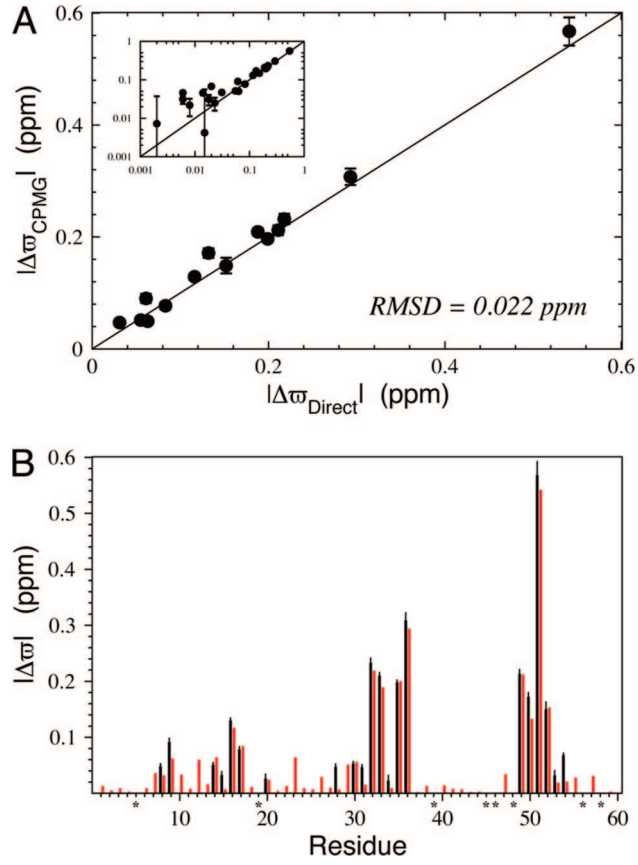

Figure 6. Correlation between $^{1}H^{\alpha}$ $|\Delta\varpi|$ values (ppm) extracted from fits of relaxation dispersion data recorded on a fractionally deuterated, uniformly ^{13}C labeled Abp1p SH3 domain sample (≈5% peptide) using the version of the pulse sequence of Figure 2 that includes the $^{1}H^{\alpha}$ reburp-refocusing element and the corresponding values measured directly from samples of free and fully bound Abp1p SH3 domains. See legend to Figure 5 for further details.

(69) Ösapay, K.; Case, D. A. *J. Biomol. NMR* **1994**, *4*, 215–230.

(70) Lundström, P.; Teilum, K.; Carstensen, T.; Bezsonova, I.; Wiesner, S.; Hansen, D. F.; Religa, T. L.; Akke, M.; Kay, L. E. *J. Biomol. NMR* **2007**, *38*, 199–212.

(71) LeMaster, D. M.; Kushlan, D. M. *J. Am. Chem. Soc.* **1996**, *118*, 9255–9264.

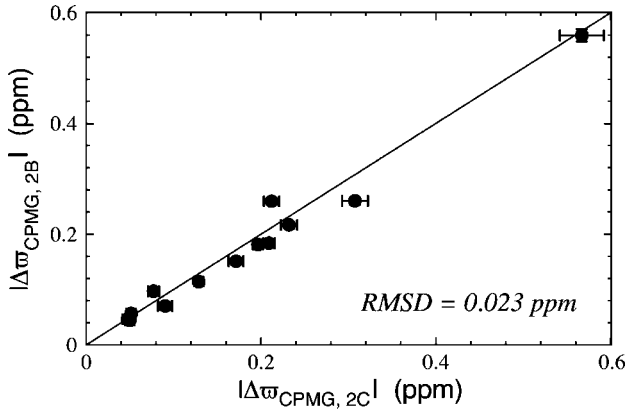

Figure 7. Correlation between $^1H^\alpha$ $|\Delta\varpi|$ values (ppm) extracted from fits of relaxation dispersion data recorded on a fractionally deuterated, uniformly ^{13}C labeled Abp1p SH3 domain sample (~5% peptide) using the version of the pulse sequence of Figure 2 that includes the $^1H^\alpha$ *J*-refocusing element of Figure 2B (*y* axis) or the $^1H^\alpha$ selective refocusing pulse of Figure 2C (*x* axis). The solid line ($y = x$) corresponds to a perfect correlation between the two data sets. The rmsd between the two data sets is indicated in the figure.

the incorporation of label although they may lead to slower bacterial growth and lower levels of overexpression. For optimal results the carbon source should, of course, be deuterated.

As expected, there is an excellent correlation between $|\Delta\varpi|$ values extracted from fits of data measured with the pulse schemes of Figure 2B and C, as shown in Figure 7. For the 14 residue subset for which chemical shift values are obtained from both methods a pairwise rmsd of 0.023 ppm is obtained, with a maximum deviation of 0.05 ppm for Leu49. It is reassuring to note that residues with the largest shift deviations based on analysis of dispersions from one method usually were not even included in the analysis using data from the second approach since they did not "pass" the F-test described in Materials and Methods. Thus, reliable data can be extracted by using both methods even if the chemical shifts of $^{13}C^\beta$ and $^1H^\beta$ are unknown. If on the other hand they are known, it is straightforward to predict which residues are prone to artifacts and remove them from the analysis.

To establish that the methodology presented is robust over a range of exchange parameters we have repeated our analysis of the Abp1p SH3/Ark1p peptide system using a sample that is estimated to be approximately 95% bound on the basis of ^{15}N dispersion experiments. The ligated form of the SH3 domain is now the visible, ground-state but more importantly the exchange rate is increased since the pseudofirst order on-rate is proportional to the free ligand concentration, that increases as a function of total ligand added. This allows us to evaluate the performance of the experiment in faster exchange regimes. From fits of $^1H^\alpha$ dispersion profiles k_{ex} is increased approximately 3 fold (from the case where 5% ligand is added) to 1060 ± 30 s^{-1} and the population of the free state, p_B, is $5.3 \pm 0.2\%$. Due to issues of resolution in the spectrum of the bound form we could not analyze data from residues Glu14, Asp33 and Asp35 for which significant dispersion profiles were obtained from the analysis of data recorded on the 5% bound sample. However, for the 17 residues with statistically significant dispersion curves in the present case an excellent correlation between $|\Delta\varpi|$ values is obtained, Figure 8, with a pairwise rmsd of 0.034 ppm. The large deviation of 0.09 ppm for Pro51 is attributed to issues

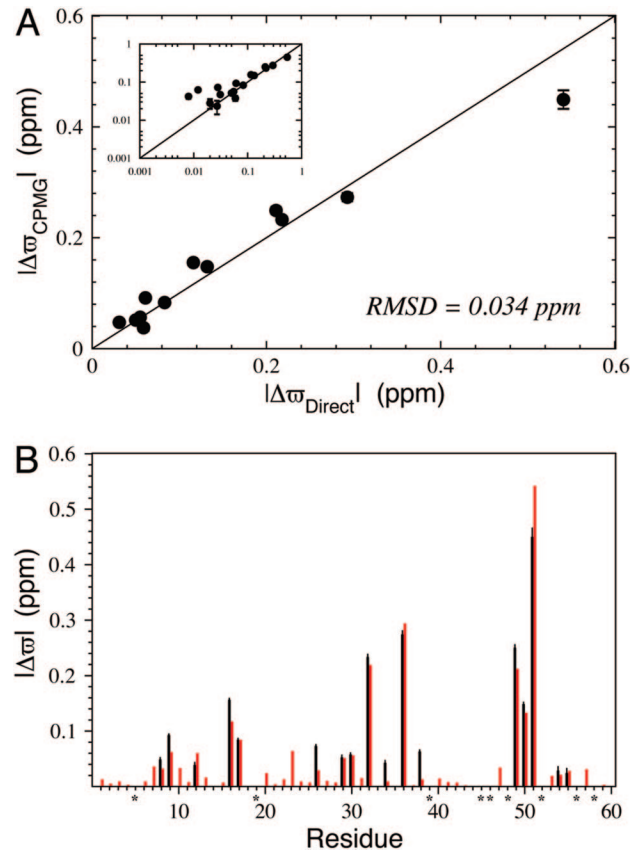

Figure 8. Correlation between $^1H^\alpha$ $|\Delta\varpi|$ values (ppm) extracted from fits of relaxation dispersion data recorded on a fractionally deuterated, uniformly ^{13}C labeled Abp1p SH3 domain sample (~95% peptide) using the version of the pulse sequence of Figure 2 that includes the *J*-refocusing element (*y* axis) and the corresponding values measured directly from samples of free and fully bound Abp1p SH3 domains (*x* axis). Other details can be found in the legend to Figure 5.

of low sensitivity, especially for small values of ν_{CPMG} and profiles recorded at 800 MHz. Note that small but measurable deviations between $|\Delta\varpi_{CPMG}|$ and $|\Delta\varpi_{Direct}|$ are obtained for Ile26, Leu38 and Leu49 as was described above for the 5% ligand bound sample.

In summary, we have shown that accurate $^1H^\alpha$ chemical shifts of invisible, excited protein states can be obtained via relaxation dispersion experiments. The effects of $^1H^\alpha-^1H^\beta$ homonuclear scalar couplings can be largely suppressed using a strategy in which fractionally deuterated proteins are produced from $U-^{13}C$, $^2H-$glucose and 50% D_2O/50% H_2O that ensures a level of deuteration of at least 50% at the C^β position and often much higher. Evolution during the CPMG pulse train from residual $^1H^\alpha-^1H^\beta$ couplings is minimized by using pulse schemes that exploit differences in chemical shifts between either $^{13}C^\alpha$,$^{13}C^\beta$ or $^1H^\alpha$,$^1H^\beta$ spins. The methodology is applied to an exchanging system that involves the binding of a peptide ligand to an SH3 domain, for which chemical shift differences of the exchanging states are known to high accuracy from separate experiments recorded on apo and ligand bound forms of the protein. It is thus possible to establish that $^1H^\alpha$ chemical shifts extracted from dispersion profiles are, on average, accurate to 0.03 ppm, an order of magnitude better than they can be predicted from structure using database programs.[42] The methodology presented is a valuable addition to a growing number of dispersion experi-

ments that will allow a detailed characterization of excited states of protein molecules.

Acknowledgment. This work was supporting by funding from the Canadian Institutes of Health Research (CIHR). We thank Ms. Hong Lin for assistance with the purification of the Ark1p peptide and Dr. Eriks Kupce (Varian Inc.) for valuable suggestions regarding implementation of adiabatic decoupling elements. P.L. and P.V hold fellowships from the CIHR Training Grant on Protein Folding in Health and Disease, while D.F.H is supported by a CIHR postdoctoral fellowship. LEK is the recipient of a Canada Research Chair in Biochemistry.

Supporting Information Available: Complete ref 31. This material is available free of charge via the Internet at http://pubs.acs.org.

JA807796A